A control- and estimation-oriented gravity separator model for oil and gas applications based upon first principles

Christoph J. Backi,* Brian A. Grimes, and Sigurd Skogestad

Department of Chemical Engineering, Norwegian University of Science and Technology (NTNU), NO-7491 Trondheim, Norway

E-mail: christoph.backi@ntnu.no

Phone: +47 944 79 561

Abstract

In this work, we introduce a simple model for a gravity separator based on first principles. It can be used for controller design to control the levels of oil, water and the gas pressure as well as observer design to estimate unmeasurable parameters and disturbances. Evaluation of separation efficiencies for the respective water- and oil-continuous phases are part of the model in addition. The model incorporates three dynamic state equations describing the levels of the overall liquid (water plus oil) and water as well as the gas pressure subject to the in- and outflow dynamics. Furthermore, algebraic equations calculating simplified droplet distributions for each continuous phase are introduced in order to determine the exchange of water and oil between the two continuous phases. The controllers are of PI-type and control the outflows of the separator. Additionally, we introduce a virtual monitoring approach for the inflows of gas and liquid as well as the effective split ratio of oil and water entering the continuous water phase. Measurements for these variables are either expensive, unreliable or even impossible to take (as for the split ratio). We demonstrate the results in simulations.

Introduction

The composition of well streams from petroleum reservoirs typically consist of different phases, such as liquid hydrocarbons (heavy oil and condensate), liquid water and gas. It is crucial and beneficial to separate these phases early in the processing stage in order to obtain as pure single-phase streams as possible for further distribution via pumps and compressors. This is usually achieved by utilizing not only one, but several separation stages in series. A first rough separation of gas, oil and water can be obtained in gravity separation devices. Further purification of the gas phase can be achieved in gas-scrubbers, which remove remaining liquid droplets from the gas. This is essential in order to avoid damages to upstream compression systems. The respective oil and water phases are treated in e.g. hydrocyclones and coalescer membranes.

In this work, we aim for a rather simple, control-oriented model of a three-phase gravity separator for bulk separation of oil, water and gas from a well stream. The main driving force for separation is the gravitational force due to differences in the specific densities of the different phases / media. A significant modeling principle is thereby *Stokes' law*, which characterizes the respective vertical settling or rising velocity v_v of a droplet dispersed in a continuous phase:

$$v_v = \frac{gD^2(\rho_d - \rho_c)}{18\mu_c}. \tag{1}$$

Here, $g \approx 9.8$ m s^{-1} is the gravitational acceleration, D [m] denotes the droplet diameter, ρ_d and ρ_c [kg m^{-3}] are the densities of the dispersed and continuous phases, respectively, and μ_c [kg m^{-1} s^{-1}] indicates the dynamic viscosity of the continuous phase. For small particles (small D), where the rising velocity v_v is too small, we may not get separation (liquid phase) or we may get entrainment (vapor phase). Despite being able to describe separation processes in a simple manner, the underlying dynamics and physical phenomena can be very complex in principle. Many different phenomena can occur in addition to sedimentation (settling of droplets) and creaming (rise of droplets), which are described by (1), such as coalescence (fusion of small droplets to

a bigger droplet) and breakage (a big droplet breaks into smaller droplets), which in turn affect the sedimentation and creaming phenomena. In addition, droplets can accumulate at interfaces between particular phases, hindering the transfer between phases and ultimately slowing down separation. These accumulation phenomena include the dense-packed / emulsion layer between the oil and water phases as well as the foaming layer between the oil and gas phases.

When it comes to previous work on modeling of gravity separator devices, most of these models lack a dynamic, control-oriented approach. Sayda and Taylor [1] suggest a modeling approach and conclude that simulations in combination with an oil production facility deliver acceptable results, despite the model's simplicity. A simulation model based on CFD (computational fluid dynamics) calculations is introduced in Hallanger et al. [2] for three-phase gravity separators. The authors come to the conclusion that entrainment of droplets depends heavily on the droplet diameter. This is not a surprise, since the separation velocity is almost proportional to the square of the droplet diameter, see (1). In his thesis, Arntzen [3] investigated an experimental pilot gravity separator subject to increasing water feeds. In addition, the author provides a detailed introduction to gravity separator functional principles. In a series of studies, Hansen et al. [4] and Hansen et al. [5] explored the fluid flow inside gravity separators divided into different zones utilizing numerical tools. The result of these simulation studies was a better understanding of the fluid flow fields in specific zones, which can be used to improve future layouts since e.g. backflows can be minimized. Laleh et al. [6] investigated the flow fields inside the Gullfaks-A three-phase gravity separator using a combined approach consisting of volume of fluid (VOF) and discrete phase model (DPM) techniques. The aim was to capture the macro- and microscopic phenomena of phase separation and the authors concluded that their study, compared to the study of Hansen et al. [5], demonstrated a realistic and reasonable overall picture of phase separation in the separator.

The present article is a contribution towards the development of more sophisticated, yet control-oriented gravity separator models, closing the gap between e.g. the work of Sayda and Taylor [1] and the aforementioned computationally demanding CFD models. By including classes of droplet sizes, we postulate that the model could reflect the sedimentation and creaming dynamics in a

separation device in a more accurate way. Control-oriented models must deliver trustworthy results to design controllers for the dynamic variables (water and overall liquid levels as well as gas pressure). Like in Backi and Skogestad[7], the present work utilizes simple PI control algorithms to operate the gravity separator within specified, safe limits. These controllers rely on level- and pressure-measurements, where the challenge does not lie in obtaining pressure measurements, but in the determination of oil and water levels. In Jaworski and Meng[8], a single-electrode capacitance probe is suggested assuming clear interfaces. However, there exist disadvantages in spatial resolution for this method and hence an array of identical probes consisting of different segments can be utilized. An ultrasonic-based device for accurate measurement of oil, emulsion and water levels is introduced by Meribout et al.[9] with the conclusion that ultrasound is reasonable both from a physics as well as from an integrated electronics point of view. Industry often uses so-called nucleonic level measurements. These provide density measurements enabling the determination of interface locations together with phase levels, as presented by e.g. McClimans and Fantoft[10]. Overviews over level measurement techniques are provided in Bukhari and Yang[11] and Hjertaker et al.[12].

In addition to enabling controller design, the developed control-oriented gravity separator model should also reliably predict purities of the respective continuous phases, especially since the measurements of oil in water and water in oil are often not reliable or even not available. A method to measure the droplet size distributions in water-in-oil emulsions has been proposed in van der Tuuk Opedal et al.[13], which relies on low-field nuclear magnetic resonance (NMR). The authors conclude that a comparison between an optical microscope reference technique and the NMR method showed good correlation and that an advantage of the NMR method was the measurement of the droplet size distribution without making assumptions on its shape. However, this method is sample-based and not available for on-line measurement. Generally, no reliable methods exist for on-line measurement of droplet size distributions. The measurement of compositions of multiphase flows can be achieved by so-called electrical resistance tomography (ERT), as described and applied in e.g. Bennett and Williams[14], Durdevic et al.[15] and Pedersen et al.[16]. The

functional principle underlying this method is the difference in electrical resistance of different substances. However, this method only works for certain flow regimes and additionally calibration might be difficult. Another method is a differential dielectric sensor model as introduced in Li et al.[17], who conclude that it agrees very well with test data, however, only for specific, well-mixed, homogeneous fluids. In a brief article, Luggar et al.[18] describe energy dispersive X-ray scatter for measurement of oil/water ratios and conclude that the methodology has great potential for multiphase flow measurement and on-line monitoring. In general, multiphase flow meters are expensive, require high maintenance and are only partially reliable. An overview on multiphase flow metering technology can be found in e.g. Thorn et al.[19].

High restrictions on the measurement and monitoring devices introduced above are imposed due to measurement noise, sensor drift and bad calibration. Therefore, not only the control-oriented modeling part is crucial for controller performance, but also the integration of measurement devices and soft sensors / virtual measurement devices.

For safe operation, it is beneficial to obtain information about different process conditions and potential disturbance variables, such as the inflows of gas and liquid as well as the split ratio of oil and gas entering the continuous water phase. Hence, a state- and parameter-observer will be designed to estimate these values for process monitoring purposes and, in addition, to obtain less noisy signals of the measured variables for control purposes. Due to its simplicity and robustness properties, a suitable algorithm for such an observer is the Extended Kalman Filter (EKF), which has been and is still used in a broad variety of applications. The rather poor accuracy of multiphase flow meters as well as of measurement devices to determine the fraction of oil in water or water in oil are good reasons to investigate the possibility of designing an observer to determine the inflows of liquid and gas as well as the (effective) split ratio.

The paper is structured as follows: First we introduce the mathematical model, which is derived from first principles. Thereafter the controller design is presented, followed by simulation results. The paper is closed with concluding remarks and an outlook on future work.

Mathematical Model

This paper introduces a simple modeling approach based on *Stokes' law* (1) for different classes of droplet sizes as a static, algebraic part of the model. This means that only sedimentation and creaming will be regarded. Coalescence and breakage will potentially be included in later stages, ideally incorporating population balance equations (PBEs). Furthermore, no dense-packed (emulsion) layer is considered at the oil-water-interface and the droplets are assumed to directly leave into their respective bulk phases at this interface. An assumption of this type makes it necessary that the rate of interfacial coalescence is less than the flux of droplets to the interface between phases by sedimentation or creaming. It can be regarded reasonable under operating conditions, where an effective demulsifier is properly dosed to the separator inlet stream. Besides the above assumptions, the following simplifications are adopted:

- No gas droplets are found in the liquid phases as well as no liquid droplets in the gas phase (no entrainment)
- Plug flow inside the separator with a different velocity for each phase in the horizontal direction, including droplets
- Instant levelling of water and liquid levels with respect to changes of in- and outflows, that is, friction loss is neglected in the horizontal direction

The dynamic part of the model regards changes of the gas pressure as well as the overall liquid level (water plus oil) and the water level. Mainly due to the cylindrical shape of the gravity separator, these parts of the model are nonlinear. The volumetric three-phase inflow into the separator depicts a disturbance variable, whereas the outflows for gas, oil and water are the manipulated variables. The algebraic part of the model consists of a simple calculation of the droplet distribution inside the active separation zone. Thereby, distributed and static particle size classes are assumed. The purpose of the model is to control the pressure of the gas as well as the levels of liquid and water and to predict the amounts of water in oil and oil in water for each of the two respective bulk phase outflows.

In Figure 1 a simplified schematic of the gravity separator is displayed, including a cross sectional view on the left side. It illustrates the liquid and water levels, the different cross sectional areas and the dimensions of the separator as well as the positions of the in- and outlets. It should be mentioned that there exist several different types of equipment for the inlet in order to achieve a first rough separation of the incoming multiphase stream. These include, but are not limited to, dish-heads (shown here), cyclonic devices, diverter plates or vane-inlets as described in e.g. Bothamley[20]. Before the gas is released through the outlet, typically a preceding demister removes liquid droplets from the gas stream. In between the dashed lines in Figure 1, we define the active separation zone with length L. After a first rough separation in the turbulent inlet zone of the separator, the flow is assumed uniform in each phase when it enters the active separation zone, where we consider continuous water and oil levels to have formed such that droplet balances can be calculated for each phase. The liquid inflow enters the separator with a water cut α and an oil cut $1-\alpha$, which denote the respective fractions of water and oil in the inlet stream. However, not all the water is found in the bulk water volume as it enters the separation zone, but a fraction of it will disperse into the bulk oil volume. The same holds for the inflowing oil, which will partly end up in the bulk water phase. Therefore, we define four fractions, namely ϕ_o, which is the fraction of inflowing oil going into the oil phase, ϕ_w representing the fraction of inflowing water going into the water phase, $1-\phi_o$ giving the fraction of inflowing oil going into the water phase and $1-\phi_w$ defining the fraction of the water going into the oil phase. Hence, the inflow into the continuous water phase can be described as

$$\begin{aligned} \underbrace{q_{W,in}}_{\substack{\text{total inflow into}\\ \text{continuous water phase}}} &= \underbrace{q_{L,in}(\alpha\phi_w)}_{\substack{\text{total water into}\\ \text{continuous water phase}}} + \underbrace{q_{L,in}(1-\alpha)(1-\phi_o))}_{\substack{\text{total oil into}\\ \text{continuous water phase}}}, \\ &= q_{L,in}\underbrace{(\alpha\phi_w+(1-\alpha)(1-\phi_o))}_{\gamma}, \end{aligned} \tag{2}$$

where the split ratio γ is the fraction of total liquid inflow $q_{L,in}$ entering the continuous water phase.

The geometrical specifications of the considered gravity separator correspond roughly with those of the Gullfaks-A separator, see Laleh et al.[21], Figure 1.

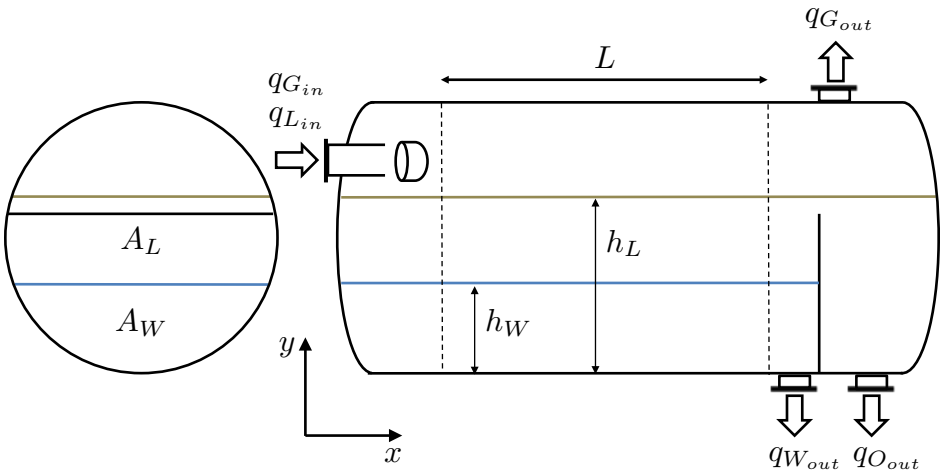

Figure 1: Simplified schematic of the gravity separator

Note that the water outlet is assumed to be a mixture of all liquid in the water-continuous phase leaving the active separation zone. In effect, this means that there is no dead volume in the outlet zone. The same applies to the oil-continuous phase at the outlet.

Total liquid level rate of change

We assume constant liquid density and hence can express the rate of change in the separator liquid volume as

$$\begin{aligned} \frac{dV_L}{dt} &= q_{L,in} - q_{L,out}, \\ \text{with} \quad q_{L,out} &= q_{W,out} + q_{O,out}, \end{aligned} \tag{3}$$

where q_i denote the in- or outflows of liquid (L), water (W) or oil (O). We have $A_L = \frac{V_L}{L}$ and hence $\frac{dA_L}{dt} = \frac{dV_L}{dt}\frac{1}{L}$ with L being the length of the active separation zone. A_L defines the area of a circular segment with sagitta (height) h_L, which can be calculated as

$$A_L = \frac{r^2}{2}\left[2\arccos\left(\frac{r-h_L}{r}\right) - \sin\left(2\arccos\left(\frac{r-h_L}{r}\right)\right)\right], \tag{4}$$

with r denoting the radius of the separator. Differentiating (4) with respect to time yields

$$\frac{dA_L}{dt} = \frac{dh_L}{dt}\left[r^2\left(\frac{1-\cos\left(2\arccos(\frac{r-h_L}{r})\right)}{\sqrt{h_L(2r-h_L)}}\right)\right],$$

which ultimately leads to a differential equation for the liquid level h_L

$$\begin{aligned}\frac{dh_L}{dt} &= \frac{dV_L}{dt}\frac{\sqrt{h_L(2r-h_L)}}{r^2L\left(1-\cos\left(2\arccos(\frac{r-h_L}{r})\right)\right)} \\ &= \frac{dV_L}{dt}\frac{1}{2L\sqrt{h_L(2r-h_L)}}.\end{aligned} \tag{5}$$

Water level rate of change

The in- and outflow of the water phase can be calculated following the calculations for the total in- and outflow of liquid in (3), which gives

$$\frac{dV_W}{dt} = q_{W,in} - q_{W,out}$$

where $q_{W,in}$ is defined in (2). The determination of the differential equation of the water level follow the same principles as presented before, namely by defining $\frac{dA_W}{dt} = \frac{dV_W}{dt}\frac{1}{L}$ with

$$A_W = \frac{r^2}{2}\left[2\arccos\left(\frac{r-h_W}{r}\right) - \sin\left(2\arccos\left(\frac{r-h_W}{r}\right)\right)\right]$$

and its time-derivative

$$\frac{dA_W}{dt} = \frac{dh_W}{dt}\left[r^2\left(\frac{1-\cos\left(2\arccos(\frac{r-h_W}{r})\right)}{\sqrt{h_W(2r-h_W)}}\right)\right].$$

This leads to a differential equation for the water level

$$\begin{aligned}\frac{dh_W}{dt} &= \frac{dV_W}{dt}\frac{\sqrt{h_W(2r-h_W)}}{r^2L\left(1-\cos\left(2\arccos(\frac{r-h_W}{r})\right)\right)} \\ &= \frac{dV_W}{dt}\frac{1}{2L\sqrt{h_W(2r-h_W)}}.\end{aligned} \tag{6}$$

Pressure rate of change

We assume ideal gas behavior $pV_G = n_G RT$ for constant temperature. The mass balance for the gas phase yields

$$\frac{dn_G}{dt} = \frac{\rho_G}{M_G}\left(q_{G,in} - q_{G,out}\right) \tag{7}$$

and the change in gas volume is given by the negative change in liquid volume

$$\frac{dV_G}{dt} = -\frac{V_L}{dt} = -\left(q_{L,in} - q_{L,out}\right). \tag{8}$$

The time-derivative of the ideal gas law yields

$$\frac{dp}{dt}V_G + p\frac{dV_G}{dt} = RT\frac{dn_G}{dt},$$

where $V_G = V_{Sep} - V_L$. Here, V_{Sep} denotes the volume of the active separation zone and $V_L = A_L L$ is the volume of the liquid in the active separation zone. From the gas mass balance (7) and the change in gas volume (8), the pressure dynamics can be written as

$$\frac{dp}{dt} = \frac{RT\frac{\rho_G}{M_G}\left(q_{G,in} - q_{G,out}\right) + p\left(q_{L,in} - q_{L,out}\right)}{V_{Sep} - A_L L}, \tag{9}$$

where R is the universal gas constant, T denotes the temperature, ρ_G indicates the gas density, M_G is the molar mass of the gas and $q_{G,in}$ and $q_{G,out}$ give the respective in- and outflows of gas.

Simplified Droplet Balances

In order to develop a more accurate droplet balance calculation and to render the model ready for future implementations of coalescence and breakage, the volume of the active separation zone is divided into N_S volumetric segments along its x-direction. Thereby, (5) and (6) are calculated for each segment and averaged over the number of segments. In the same fashion, the respective in- and outflows are divided by the number of segments and added to / subtracted from each segment's dynamic equation. This has the consequence that there exist no delays concerning the increased or decreased throughput of liquid along the separator's length. In Figure 2, a simplified schematic of the evolution over five volumetric segments is depicted.

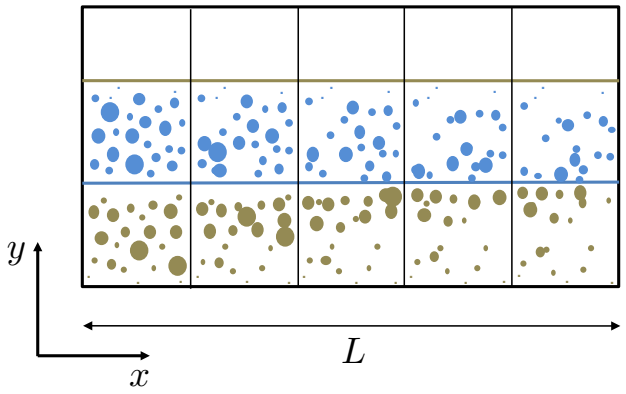

Figure 2: Simplified schematic of the assumed droplet distribution and evolution over the length of the active separation zone

For now, due to the fact that the model doesn't consider any coalescence and breakage of droplets, we base the calculations on a static droplet size distribution. We define 500 classes of droplet sizes, evenly distributed between 0 and 1000 µm, hence $c_i = \{2,4,6,\ldots,1000\}$ µm, $i = 1,2,\ldots,500$. The droplet balance calculations are now based on the following assumptions

- The horizontal velocity of the droplets is equal to the velocity of the respective phase (volumetric inflow divided by the respective cross sectional area)
- The velocity of the droplets in vertical direction is determined by *Stokes' law* (1) without regarding a decelerating correction factor as introduced in e.g. Richardson and Zaki [22].
- The droplets present at the end of the final volumetric segments (right hand side) leave the separator directly through the respective outlets of the bulk phases.

The horizontal residence times t_h of a droplet size class in each volumetric segment of the separator can be calculated as

$$\begin{aligned} t_{h_W} &= \frac{L}{N_S}\frac{A_W}{q_W}, \\ t_{h_O} &= \frac{L}{N_S}\frac{A_O}{q_O}, \end{aligned} \tag{10}$$

where $\frac{L}{N_S}$ defines the length of a volumetric segment, A_j represent the areas of the circular segments of water or oil, respectively, and q_j are the volumetric inflows into the respective continuous phases. Ultimately, the horizontal residence times in (10) will be compared to the vertical residence time derived from (1)

$$t_{v_i} = \begin{cases} \frac{h_W}{v_{v_i}} = \frac{18\mu_O}{gc_i^2(\rho_W-\rho_O)}h_W & \text{for oil droplets in the continuous water phase} \\ \frac{h_O}{v_{v_i}} = \frac{18\mu_W}{gc_i^2(\rho_O-\rho_W)}h_O & \text{for water droplets in the continuous oil phase} \end{cases}$$

where h_j indicate the levels of water or oil, respectively ($h_O = h_L - h_W$), and c_i denotes the diameter of droplet size class i. If a droplet size class reaches the water-oil-interface before reaching the next volumetric segment, the respective volume is added to its respective bulk phase and subtracted from the phase it was dispersed in.

The calculations for the respective droplet classes are modeled in terms of their positions relative to the water-oil-interface. Based on these positions compared to the positions of the same droplet class in the previous volumetric segment, the number of droplets and consequently the volume leaving the continuous phase can be calculated as a sum over all droplet classes. The calculations are based upon simple *if–else* statements, in the following presented for dispersed oil droplets in the continuous water phase (the calculations are the same for dispersed water droplets in the continuous oil phase):

Let the segment of interest be segment $m \in N_S$

for $i = 1 : 500$

if $t_{h_W} < t_{v_i}$

$$pos_i^{segment\ m} = t_{h_W} v_{v_i} + pos_i^{segment\ m-1}$$

$$n_i^{into\ segment\ m+1} = n_i^{from\ segment\ m-1} \left(1 - \frac{t_{h_W} v_{v_i}}{h_W - pos_i^{segment\ m-1}} \right)$$

$$V_i^{into\ oil\ phase} = n_i^{from\ segment\ m-1} V_i^{droplet} \frac{t_{h_W} v_{v_i}}{h_W - pos_i^{segment\ m-1}}$$

else

entire volume of droplet class i goes into its bulk phase

end

end

where $pos_i^{segment\ m}$ gives the position of droplet class i at the end of segment m, $t_{h_W} v_{v_i}$ describes

the vertical distance droplet class i travels in one segment of length $\frac{L}{N_S}$ and $n_i^{into\ segment\ m+1}$ depicts the amount (number) of droplets of class i that leave segment m into segment $m+1$, but remain dispersed in the continuous phase. Accordingly, $n_i^{from\ segment\ m-1}$ represents the droplets that have not been separated in segment $m-1$, and hence remain dispersed in the continuous phase in segment m. $V_i^{into\ oil\ phase}$ is the volume of droplets of class i that leave segment m into their bulk (oil) phase and $V_i^{droplet} = \frac{\pi}{6}c_i^3$ defines the volume of one droplet of class i. A volumetric flow is obtained by dividing the respective volume by the residence time, in this case t_{h_W}.

Initial distribution The droplet size distributions of the oil- and water-continuous layers in the inlet zone of the separator represent the boundary condition of the model presented above at $x = 0$. In a real separator, well fluid streams containing gas, oil and water enter a gravity separator through an inlet section characterized by high turbulence and mixing. This turbulent inlet section is usually isolated from the main separation chamber by the installation of an internal flow dampener. The extent of turbulence and mixing in the inlet section depend on many factors such as design geometry, flow regime (dispersed flow, stratified flow, etc.), pressure, etc. An advanced CFD simulation[2,23] of the turbulence and mixing would be too cumbersome for the purposes of the model presented above. Consequently, we idealize the inlet section of the separator as a "flash" separation followed by two continuous stirred-tank reactors (CSTRs) as shown in Figure 3.

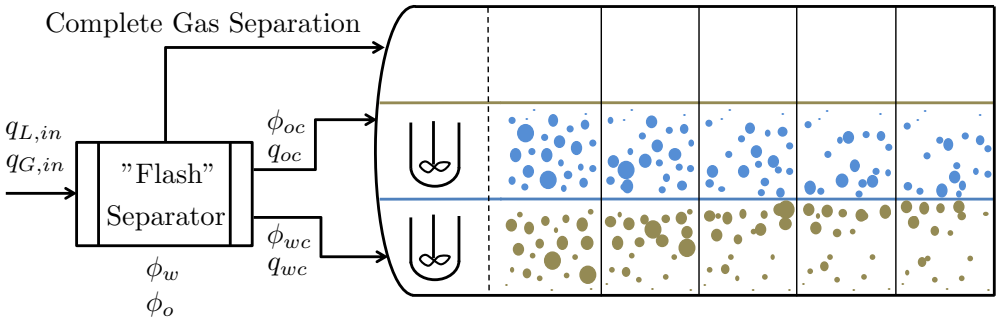

Figure 3: The inlet zone of the gravity separator with the considered CSTRs for each continuous phase

In this abstract idealization, the three phase well fluid with water cut α is fed into a "flash" separator where the gas is considered to completely separate and exit to the active separation zone.

The oil and water streams mix and partition in the “flash” separator and the mixing of oil-into-water and water-into-oil are characterized by the initial separation factors ϕ_w and ϕ_o, respectively. It should be noted that ϕ_w and ϕ_o will most likely be functions of the inlet flow rate, flow regime, and inlet section geometry. Along with the gas stream, a water continuous dispersion (index wc) and an oil continuous dispersion (index oc) with known dispersed phase volume fractions

$$\phi_{wc} = \frac{(1-\alpha)(1-\phi_o)}{(1-\alpha)(1-\phi_o)+\alpha\phi_w},$$
$$\phi_{oc} = \frac{\alpha(1-\phi_w)}{\alpha(1-\phi_w)+(1-\alpha)\phi_o},$$

exit the “flash” separator. Each stream is fed into a CSTR, which represent the turbulent water- and oil-continuous layers in the inlet section. The CSTR layers are characterized by their volumes, V_i ($i = wc, oc$), which are determined from the current total liquid level h_L and water level h_W, along with their turbulent kinetic energy dissipation rate, ε_i ($i = wc, oc$). The turbulent kinetic energy dissipation rate ε_i along with the dispersed volume fraction in each CSTR, ϕ_i, will be the main factors in establishing the droplet size distribution in each layer of the inlet section.

It should be noted that the "flash" separation is simply an idealization of how the inlet flow is distributed to the oil and water continuous layers. By considering that the inlet gas is separated from the liquid phase, the purpose of the "flash" conceptualization is to determine the inlet flow rates, $q_{O,in}$ and $q_{W,in}$, and compositions, ϕ_{oc} and ϕ_{wc}, to the oil- and water-continuous layers in order to solve the population balance model for the droplet size distribution in each layer. Therefore, for a given inlet liquid flow rate, $q_{L,in}$, water cut, α, and split factors ϕ_o and ϕ_w, the volume fractions ϕ_{oc} and ϕ_{wc} of droplets in each layer is determined and the population balance model for the inlet section is solved. We consider $q_{L,in}$, α, ϕ_o and ϕ_w, to be constant for each simulation case, so these calculations are done once to establish the boundary conditions for the dynamic system model, but are not dynamically solved in the controller and observer models.

Assuming that the volume V_i of each CSTR layer is effectively constant during the droplet

residence time and that the turbulence in each CSTR layer is isotropic, in the inertial sub-range of the energy spectrum, and uniform throughout the volume V_i, a dynamic population balance for this system can be written as follows (Jakobsen[24], Grimes[25], Grimes et al.[26]):

$$\begin{aligned}\frac{\partial f_{n,i}(t,r)}{\partial t} = &\underbrace{\int_0^{\frac{r}{\sqrt[3]{2}}} r_{c,i}(r',r'')f_{n,i}(t,r')f_{n,i}(t,r'')dr'}_{\text{coalescence birth term}} - \underbrace{f_{n,i}(t,r)\int_0^{\infty} r_{c,i}(r,r')f_{n,i}(t,r')dr'}_{\text{coalescence death term}} \\ &+ \underbrace{\int_r^{\infty} 2g_i(r')\beta(r,r')f_{n,i}(t,r')dr'}_{\text{breakage birth term}} - \underbrace{g_i(r)f_{n,i}(t,r)}_{\text{breakage death term}}, \quad \forall t>0,\ V_i, i = wc, oc\end{aligned} \tag{11}$$

where $r'' = (r^3 - r'^3)^{\frac{1}{3}}$, t is the time variable [s], r denotes the droplet radius coordinate [m] and $f_{n,i}$ represents the droplet number density distribution for layer i [m^{-4}]. The droplet number density distribution is defined such that integrating the product of f_n and the corresponding drop volume will yield the inlet dispersed phase volume fraction for each layer

$$\phi_i = \int_0^{\infty} \frac{4\pi}{3} r'^3 f_{n,i}(t,r')dr', \quad \forall t>0,\ V_i, i = wc, oc$$

The function $r_{c,i}(r,r')$ in (11) represents the swept volume rate of coalescence [$m^3\ s^{-1}$] (Jakobsen[24], Grimes[25], Grimes et al.[26]) between two droplets of size r and r' in CSTR layer i. Typically (see e.g. Jakobsen[24], Grimes[25], Grimes et al.[26], Prince and Blanch[27], Chesters[28], Coulaloglou and Tavlarides[29], Vankova et al.[30]), r_{ci} is determined by the product of a droplet collision rate function, ω_i, and a probability of coalescence for each collision, Φ_i. The collision rate function, ω_i, considers collisions to occur mainly through the fluctuating turbulent velocity of the liquid phase as given in Prince and Blanch[27]. The probability of coalescence for each collision, Φ_i, is obtained from the ratio of the film drainage time to the droplet contact time as given in Chesters[28]. The equations composing the swept volume rate of coalescence, r_c, for two droplets of size r and r' are given by

$$r_{c,i}(r,r') = \omega_i(r,r')\Phi_i(r,r'), \quad i = wc, oc$$

$$\omega_i(r,r') = k_{c1,i} 4\sqrt[3]{2}\varepsilon_i^{\frac{1}{3}}(r+r')^2\left[r^{\frac{2}{3}} + r'^{\frac{2}{3}}\right]^{\frac{1}{2}}, \quad i = wc, oc$$

$$\Phi_i(r,r') = \exp\left[-k_{c2,i}\frac{\rho_{c,i}^{\frac{1}{2}}\varepsilon_i^{\frac{1}{3}}}{2^{\frac{1}{6}}\sigma^{\frac{1}{2}}}\left(\frac{1}{2}\frac{rr'}{r+r'}\right)^{\frac{5}{6}}\right], \quad i = wc, oc,$$

where ε_i denotes the turbulent kinetic energy dissipation rate per unit mass in CSTR layer i [m^2 s^{-3}], $\rho_{c,i}$ represents the density of the continuous phase in CSTR layer i [kg m^{-3}], and σ denotes the interfacial tension between the oil and water phases [N m^{-1}]. The proportionality constants $k_{c1,i}$ and $k_{c2,i}$ are constants used to fit experimental data or tune the model for CSTR layer i. The function $g_i(r)$ in (11) represents the breakage rate for a droplet of size r in CSTR layer i. The breakage rate function used in this work is taken from Coulaloglou and Tavlarides[29] and considers breakage to occur when the turbulent energy supplied to a droplet by an eddy exceeds the droplet's surface energy. The function $\beta(r,r')$ in (11) denotes the probability of obtaining a droplet of size r when a droplet of size r' breaks and is taken from the expression developed by Vankova et al.[30]. It should be noted that the function β will be the same for both CSTR layers since it does not include any physical constants. The breakage kernel functions are as follows

$$g_i(r) = k_{b1,i}\frac{\varepsilon^{\frac{1}{3}}}{2^{\frac{2}{3}}r^{\frac{2}{3}}}\sqrt{\frac{\rho_{d,i}}{\rho_{c,i}}}\exp\left[-k_{b2,i}\frac{\sigma}{2^{\frac{5}{3}}\rho_{d,i}\varepsilon_i^{\frac{2}{3}}r^{\frac{5}{3}}}\right], \quad i = wc, oc$$

$$\beta(r,r') = 7.2\frac{r^2}{r'^3}\exp\left[-4.5\frac{\left(2r^3 - r'^3\right)^2}{r'^6}\right]$$

with $\rho_{d,i}$ representing the density of the dispersed phase in CSTR layer i [kg m^{-3}], while $k_{b1,i}$ and $k_{b2,i}$ are constants used to fit experimental data or tune the model for CSTR layer i.

The proportionality constants, k_{c1}, k_{c2}, k_{b1} and k_{b2}, are used to tune the droplet collision rate function, ω_i, the probability of coalescence for each collision, Φ_i, and the breakage rate function,

g_i, to specific crude-oil water systems. Therefore, the nominal values of these proportionality constants are very important to provide the link between the idealized physical mechanisms used to derive ω_i, Φ_i, and g_i and the real dynamic behavior of crude-oil water emulsions. Selection of the appropriate functional forms for ω_i, Φ_i, and g_i along with the determination of their corresponding proportionality constants, k_{c1}, k_{c2}, k_{b1} and k_{b2}, for six different crude-oil water systems is the subject of ongoing research and will be reported in the near future. Specifically, we are currently performing batch CSTR experiments on oil-in-water emulsions using six different crude oils and following the dynamic evolution of the droplet volume density distribution online with a Mastersizer attached to a closed sampling loop. Regression strategies for the dynamic data sets along with analysis of parameter correlation and the error associated with the estimation of the turbulent kinetic energy dissipation rate, ε_i, will be the main focus.

An arbitrary initial distribution is chosen for each CSTR layer i and the systems are simulated over the residence time of each CSTR layer, $t_{fi} = \dfrac{V_i}{q_i}$, where $q_{wc} = q_{W,in}$ and $q_{oc} = q_{L,in} - q_{W,in}$. Numerous simulations have shown that the steady state number density distribution of a dispersion in a CSTR is independent of the initial condition, and thus, this approach should apply if the dynamics of coalescence and breakage are sufficiently fast compared to the CSTR residence time. The equations are solved by orthogonal collocation of the radial (droplet size) domain and time integration with Gear's BDF method, see Grimes [25], Grimes et al. [26].

For constant water cut α and initial separation factors ϕ_w and ϕ_o, the shape of the initial distribution does not change. That means that, if the levels of oil and / or water change, or if the liquid inflow changes value, also the residence time in the inlet zone will change, which will cause the initial distribution to be scaled by a factor in order to account for the longer or shorter hold up in the inlet zone.

These factors can be calculated via the relation

$$
\begin{aligned}
F_W &= t_{h_O}^{inlet}\left[\alpha\left(1-\phi_w\right)\right] q_{L,in}\frac{1}{V_W}, \\
F_O &= t_{h_W}^{inlet}\left[\left(1-\alpha\right)\left(1-\phi_o\right)\right] q_{L,in}\frac{1}{V_O},
\end{aligned}
\tag{12}
$$

where $t_{h_O}^{inlet}$ and $t_{h_W}^{inlet}$ are the residence times of droplets in the inlet zone of the separator in the respective water- and oil-continuous phases, and $V_O = \sum_i n_i^O V_i^O$ as well as $V_W = \sum_i n_i^W V_i^W$ are the volumes calculated by solving the PBE.

Controller and Observer Design

We here describe the controllers and observer used to control the gravity separator's dynamic states, namely the liquid and water levels, h_L and h_W, as well as the pressure p. The observer also estimates the disturbance variables $q_{L,in}$, $q_{G,in}$ and the parameter γ.

PI Controller

We apply three PI controllers to control the three dynamic states. The PI control algorithms are defined in the form

$$
K(s) = K_p + T_I\frac{1}{s},
$$

where the parameters K_p and T_I are shown in Table 1. The parameters of the PI controllers were found by applying the SIMC (*Skogestad-IMC*) tuning rules, as suggested in Skogestad[31]. The chosen values of the tuning parameter τ_c for the three PI controllers are also shown in Table 1. The states can be interpreted as pure integrating processes without time delay. Hence, an open loop step response investigation gave the controller parameters listed in Table 1.

The PI controllers do not directly use the noisy measurements of the state variables, but rather

the filtered ones from the observer, which will be introduced in the observer design section following this section. The outputs of the PI controllers correspond directly to the desired volumetric flows of oil, water and gas, respectively. To render this more realistic, the controller outputs are upper and lower bounded as well as limited in its rate of change. The lower bounds for all control signals are set to 0 $m^3\ s^{-1}$, as only flows out of the separator are allowed, whereas the upper bounds are set to 1 $m^3\ s^{-1}$. The rates of change are set to $\pm 0.05\ m^3\ s^{-2}$ to regard for actuation dynamics. Because of the bounds, anti-windup is used for the three controllers.

Table 1: Parameters for the three PI controllers

	τ_c	K_P	T_I
water level	5 s	6.49	0.325
liquid level	5 s	5.063	0.253
pressure	5 s	0.0541	0.0027

The oil-in-water and water-in-oil fractions at the respective outlets can be controlled indirectly by the levels of liquid and water in the separator. It holds that for a decrease in volumetric inflow the horizontal velocity will decrease (assumed that the respective level is constant) and thus the residence time will increase, such that the outlets of water and oil will become purer. However, throttling the inflow to the separator is not desired since it will limit production and is also not part of this investigation.

Observer design for virtual inflow monitoring

We aim for an observer design that delivers less noisy signals of the measured state variables and, in addition, estimates the disturbance variables (inflows of gas and liquid) as well as the split ratio if oil and water entering the continuous water phase, γ. The design presented here is an extension to the one already presented in Backi and Skogestad[32]. We introduce a cascaded dual observer design, where we utilize two Extended Kalman Filters. If we look at the system dynamics , we can see that the liquid level does affect the gas pressure, but not vice versa. Therefore, we can decouple the estimation of h_L and $q_{L,in}$ from the estimation of h_W, p, $q_{G,in}$ and γ leading to two observer

designs for each of the aforementioned sets of variables.

In Figure 4, a schematic of the cascaded observer design is demonstrated together with the model of the plant representing the real system.

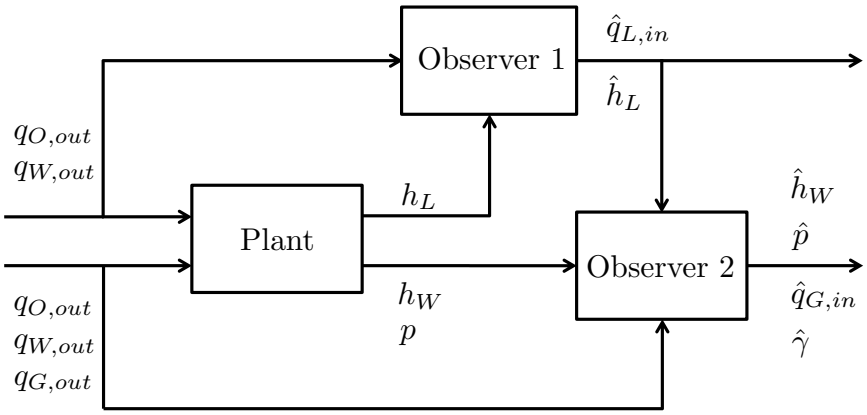

Figure 4: Schematic of the cascaded observer design in combination with the plant model

The block 'Plant' is composed of equations (5)–(9). The block 'Observer 1' is an Extended Kalman Filter and its schematic can be seen in Figure 5.

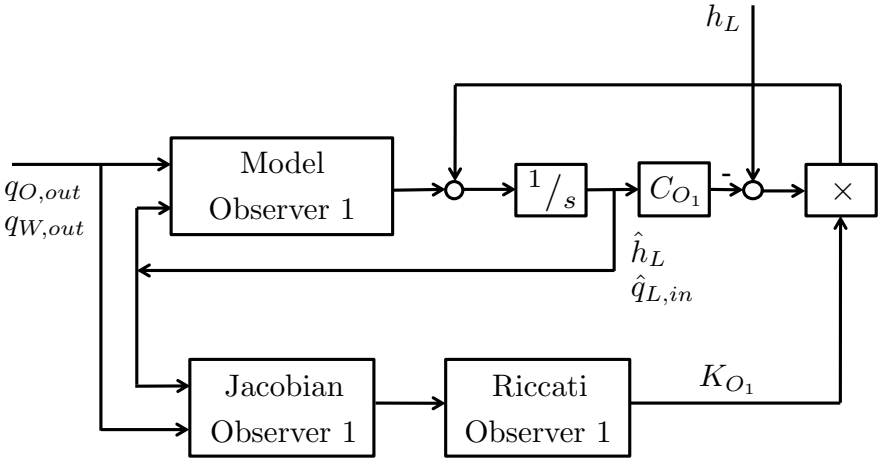

Figure 5: Schematic of Observer 1

The block 'Model Observer 1' contains the following model equations

$$\begin{aligned}\frac{d\hat{h}_L}{dt} &= f_{1,O_1} = \frac{\hat{q}_{L,in} - q_{W,out} - q_{O,out}}{2L\sqrt{\hat{h}_L(2r-\hat{h}_L)}} + w_{1,O_1}(t),\\ \frac{d\hat{q}_{L,in}}{dt} &= f_{2,O_1} = w_{2,O_1}(t)\end{aligned} \tag{13}$$

and hence the state vector is $\hat{x}_{O_1} = \begin{bmatrix}\hat{h}_L & \hat{q}_{L,in}\end{bmatrix}^T$ with the output vector $C_{O_1} = \begin{bmatrix}1 & 0\end{bmatrix}$ and the dynamics of Observer 1

$$\frac{d\hat{x}_{O_1}}{dt} = f_{O_1}(\hat{x}_{O_1}, u) + K_{O_1}(t)(y_{O_1} - C_{O_1}\hat{x}_{O_1}).$$

The partial derivatives of the observer state equations (13) with respect to the state vector $\hat{x}_{O_1}$ are computed and updated at every time iteration and included in the block 'Jacobian Observer 1'. The single entries in the matrix A_{O_1} give quite complex terms and the details are omitted, but its shape is

$$A_{O_1}(t) = \left(\frac{\partial f_{i,O_1}}{\partial \hat{x}_{j,O_1}}\right)_{i=1,\ldots,2;\ j=1,\ldots,2} = \begin{bmatrix}A^{11}_{O_1}(t) & A^{12}_{O_1}(t)\\ 0 & 0\end{bmatrix} \tag{14}$$

The Jacobian (14) is used to solve the differential Matrix-Riccati-Equation in the block 'Riccati Observer 1' at each time instant to calculate the time-varying Kalman observer gain matrix $K_{O_1}(t)$

$$\begin{aligned}\frac{dP_{O_1}(t)}{dt} &= A_{O_1}(t)P_{O_1}(t) + P_{O_1}(t)A^T_{O_1}(t) - \lambda_{O_1}P_{O_1}(t)C^T_{O_1}R^{-1}_{O_1}C_{O_1}P_{O_1}(t) + \lambda_{O_1}P_{O_1}(t),\\ K_{O_1}(t) &= \lambda_{O_1}P_{O_1}(t)C^T_{O_1}R^{-1}_{O_1},\end{aligned} \tag{15}$$

where $R_{O_1} = \mathrm{cov}\{v(t)v^T(t)\} = r_{O_1}$ is a scalar representing the covariance of the measurement noise $v_{O_1}(t)$. We do not assume covariance between process and measurement noises, which enter the system in the following way

$$\frac{d\hat{x}_{O_1}}{dt} = f(\hat{x}_{O_1}, u_{O_1}) + w_{O_1}(t),$$
$$y_{O_1} = C_{O_1}\hat{x}_{O_1} + v_{O_1}(t),$$

where u_{O_1} is the vector of manipulated variables $q_{O,out}$ and $q_{W,out}$. It must be mentioned that (15) is not of standard kind, but an implementation of a Riccati differential equation with a forgetting factor. The principles behind this design were introduced as a least squares observer including a forgetting factor in Johnstone et al.[33] with further developments in the works of Hammouri and De Leon Morales[34] and Haring[35]. An advantage of this design is that the number of tuning variables can substantially be reduced since the process noise covariance matrix Q_{O_1} is not used, but just a sole scalar parameter λ_{O_1}.

The observability condition states that the observability matrix $\mathscr{O}_{O_1} = \begin{bmatrix} C_{O_1} \\ C_{O_1}A_{O_1}(t) \end{bmatrix}$ must have full rank for all t. For the matrix $A_{O_1}(t)$ with structure in (14), $\text{rank}(\mathscr{O}_{O_1}) = 2$ and hence full observability is ensured. A further investigation of the matrix $A_{O_1}(t)$ at steady-state conditions, meaning that inflows equal outflows, leads to the Jacobian

$$A_{O_1}^{\text{steady}}(t) = \begin{bmatrix} 0 & A_{O_1}^{12}(t) \\ 0 & 0 \end{bmatrix}, \tag{16}$$

which still leads to $\text{rank}(\mathscr{O}_{O_1}) = 2$. The only cases that could potentially lead for any of the remaining entries in (16) to be zero, are $h_L \equiv 2r$. However, the model is not designed for this case and it is unlikely to happen in normal operation. Hence, it can be concluded that Observer 1 provides full observability for any feasible operational setpoint.

Just like the block 'Observer 1', the block 'Observer 2' is an Extended Kalman Filter with its schematic in Figure 6.

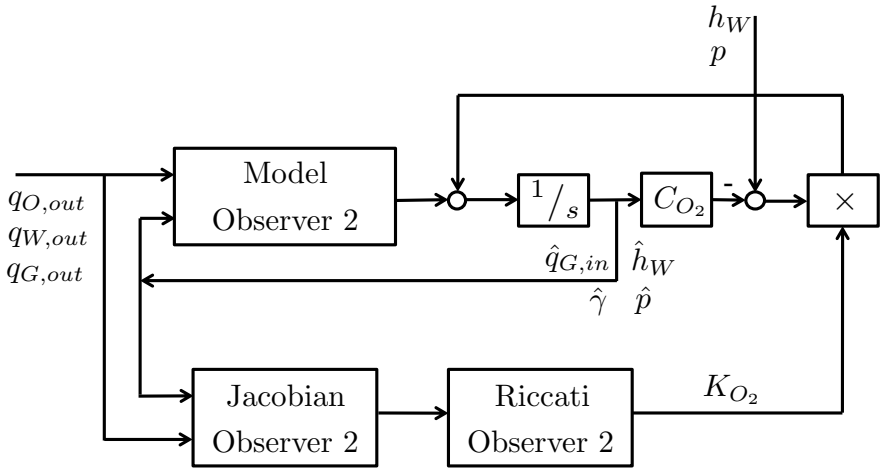

Figure 6: Schematic of Observer 2

The block 'Model Observer 1' contains the following equations

$$\begin{aligned}
\frac{d\hat{h}_W}{dt} &= f_{1,O_2} = \frac{\hat{q}_{L,in}\hat{\gamma} - q_{W,out}}{2L\sqrt{\hat{h}_W(2r-\hat{h}_W)}} + w_{1,O_2}(t), \\
\frac{d\hat{p}}{dt} &= f_{2,O_2} = \frac{RT\frac{\rho_G}{M_G}\left(\hat{q}_{G,in} - q_{G,out}\right) + \hat{p}\left(\hat{q}_{L,in} - q_{L,out}\right)}{V_{Sep} - \hat{V}_L} + w_{2,O_2}(t), \\
\frac{d\hat{q}_{G,in}}{dt} &= f_{3,O_2} = w_{3,O_2}(t), \\
\frac{d\hat{\gamma}}{dt} &= f_{4,O_2} = w_{4,O_2}(t),
\end{aligned} \tag{17}$$

where $\hat{h}_L$ and $\hat{q}_{L,in}$ are inputs delivered from 'Observer 1' and $\hat{V}_L = \hat{A}_L L$ is the liquid volume calculated with the estimated level $\hat{h}_L$, compare (4). The process noise $w_{i,O_2}(t)$ is assumed to be white noise and h_W as well as p are assumed measurable. The state vector is $\hat{x}_{O_2} = \begin{bmatrix} \hat{h}_W & p & \hat{q}_{G,in} & \hat{\gamma} \end{bmatrix}^T$ with the output matrix $C_{O_2} = \begin{bmatrix} 1 & 0 & 0 & 0 \\ 0 & 1 & 0 & 0 \end{bmatrix}$ and hence the dynamics of Observer 2 can be expressed as follows

$$\frac{d\hat{x}_{O_2}}{dt} = f_{O_2}(\hat{x}_{O_2}, u) + K_{O_2}(t)(y_{O_2} - C_{O_2}\hat{x}_{O_2}).$$

Just as for 'Observer 1', the partial derivatives of the observer equations (17) with respect to the

state vector $\hat{x}_{O_2}$ are calculated and updated at every time iteration in the block 'Jacobian Observer 2'

$$A_{O_2}(t) = \left(\frac{\partial f_{i,O_2}}{\partial \hat{x}_{j,O_2}} \right)_{i=1,\ldots,4;\ j=1,\ldots,4} = \begin{bmatrix} A_{O_2}^{11}(t) & 0 & 0 & A_{O_1}^{14}(t) \\ 0 & A_{O_2}^{2}(t) & A_{O_2}^{23}(t) & 0 \\ 0 & 0 & 0 & 0 \\ 0 & 0 & 0 & 0 \end{bmatrix}. \tag{18}$$

The differential Matrix-Riccati-Equation defined in block 'Riccati Observer 2' is solved at each time instant to calculate the time-varying Kalman observer gain matrix $K_{O_2}(t)$ using the Jacobian (18)

$$\begin{aligned} \frac{dP_{O_2}(t)}{dt} &= A_{O_2}(t)P_{O_2}(t) + P_{O_2}(t)A_{O_2}^T(t) - \lambda_{O_2}P_{O_2}(t)C_{O_2}^T R_{O_2}^{-1} C_{O_2} P_{O_2}(t) + \lambda_{O_2}P_{O_2}(t), \\ K_{O_2}(t) &= \lambda_{O_2}P_{O_2}(t)C_{O_2}^T R_{O_2}^{-1}. \end{aligned}$$

It is defined in the same fashion as already introduced in (15), where now $R_{O_2} = \mathrm{cov}\{v_{O_2}(t)v_{O_2}^T(t)\} = \mathrm{diag}\left(r_{O,k}\right)$, $k = 1,2$, is the covariance of the measurement noise $v_{O_2}(t)$. Again, no covariance is assumed between process and measurement noises, which enter the system in the following way

$$\begin{aligned} \frac{d\hat{x}_{O_2}}{dt} &= f_{O_2}(\hat{x}_{O_2}, u_{O_2}) + w_{O_2}(t), \\ y_{O_2} &= C_{O_2}\hat{x}_{O_2} + v_{O_2}(t), \end{aligned}$$

with u_{O_2} denoting the vector of manipulated variables $q_{O,out}$, $q_{W,out}$ and $q_{G,out}$.

Again, the observability matrix $\mathscr{O}_{O_2} = \begin{bmatrix} C_{O_2} \\ \vdots \\ C_O A_O(t)^3 \end{bmatrix}$ must have full rank for all t. For $A_{O_2}(t)$ as in (18), $\text{rank}(\mathscr{O}_{O_2}) = 4$. In steady-state conditions, meaning that inflows equal outflows, the Jacobian (18) becomes

$$A_{O_2}(t)^{\text{steady}}(t) = \begin{bmatrix} 0 & 0 & 0 & A_{O_1}^{14}(t) \\ 0 & 0 & A_{O_2}^{23}(t) & 0 \\ 0 & 0 & 0 & 0 \\ 0 & 0 & 0 & 0 \end{bmatrix} \tag{19}$$

which still leads to $\text{rank}(\mathscr{O}_{O_2}) = 4$ for C_{O_2}. The only cases that could potentially lead for any of the remaining entries in (19) to be zero, are $h_W \equiv 2r$ and $V_L \equiv V_{Sep} \Rightarrow V_G \equiv 0$. But as mentioned above, the model is not designed for these cases and they are unlikely to happen in normal operation. Hence, it can be concluded that the model is fully observable for any feasible operational setpoint.

The static part of the model introduced before is not included in the block 'Observer Model' in order to account for some plant-observer-mismatch in simulations and since this information would not be available from a real plant.

Simulations

The gravity separator model is a differential algebraic equation (DAE) system, and is solved and simulated using MATLAB Simulink. As mentioned before, most simulation parameters, such as the geometry and production rates, are taken from Laleh et al.[21]. In simulations, the pressure state (9) is scaled to be in the unit bar and hence the equation used for the plant as well as for the observer model is

$$\frac{dp}{dt} = 10^{-5} \left(\frac{RT \frac{\rho_G}{M_G} \left(q_{G,in} - q_{G,out} \right) + 10^5 p \left(q_{L,in} - q_{L,out} \right)}{V_{Sep} - V_L} \right).$$

Simulations for initial production rates

The simulations presented in this section are based on the 1988 Gullfaks-A production rates and cover the case for the startup of the well with a water cut $\alpha = 0.135$, gas production rate $q_{G,in} = 0.456$ m^3 s^{-1}, liquid production rate $q_{L,in} = 0.59$ m^3 s^{-1}, initial water level $h_W = 1$ m and liquid level $h_L = 2.5$ m.

Figure 7 shows the initial distributions (blue) and the distributions at the respective outlets (red) for oil droplets (left plot) and water droplets (right plot) for three different initial separation factors, namely $\phi_w = \phi_o = 0.9$ (solid lines), $\phi_w = \phi_o = 0.8$ (dashed lines) and $\phi_w = \phi_o = 0.7$ (dashed-dotted lines). The levels of water and oil are held constant at their initial values (see above). As expected, for better pre-separation, meaning large values of ϕ_w and ϕ_o, the initial distributions are smaller. This can be expected, since fewer amounts of oil and water are dispersed in the respective water- and oil-continuous phases. The distributions of oil droplets at the water outlet follow the same trend for large values of ϕ_w and ϕ_o, namely that they shift towards smaller droplet diameters, meaning that the number of overall droplets and that the droplet cut-off diameter size decrease. For water droplets dispersed at the oil outlet, however, the behavior is somewhat different, where the droplet diameter cut-off size increases for better pre-separation. The reason for this lies in the residence time of droplets, which decreases for oil droplets in water with a decrease in ϕ_w and ϕ_o. In contrary, the horizontal residence time for water droplets in oil increases with a decrease in ϕ_w and ϕ_o. This can be seen in Figure 10, where the first 200 s of simulation time hold for the case presented here.

Simulations for future production rates

The following simulations cover the case of progressed lifetime of the well with a higher water cut $\alpha = 0.475$, the same gas production rate $q_{G,in} = 0.456$ m^3 s^{-1}, slightly larger liquid production

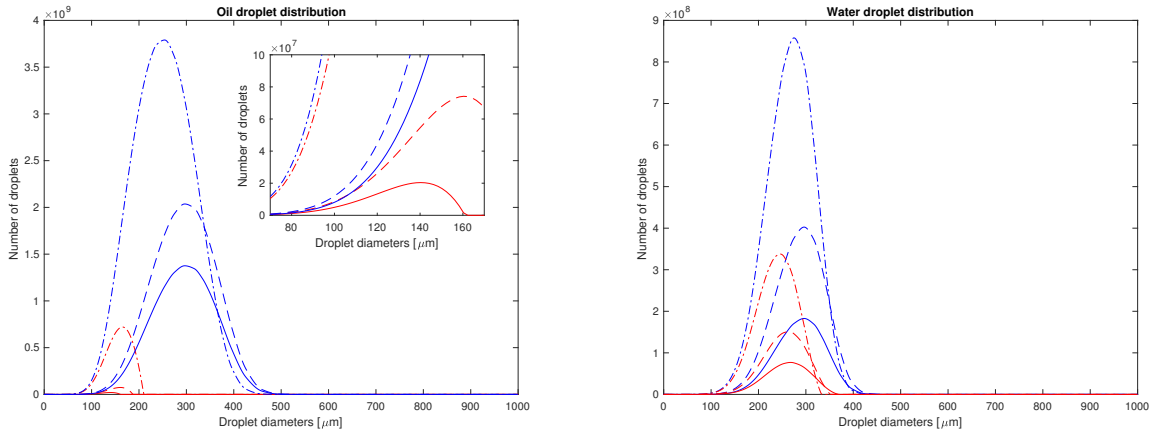

Figure 7: Initial droplet distributions (blue) and droplet distributions at the respective outlets (red) for oil droplets in water (left plot) and water droplets in oil (right plot) for three different initial separation factors ($\phi_w = \phi_o = 0.9$ (solid lines), $\phi_w = \phi_o = 0.8$ (dashed lines) and $\phi_w = \phi_o = 0.7$ (dashed-dotted lines)), low water cut

rate $q_{L,in} = 0.73$ m^3 s^{-1} and the same initial values as presented in the previous section.

Just like in Figure 7, Figure 8 shows the initial (blue) and outlet (red) distributions for oil droplets (left) and water droplets (right) for the same respective values of ϕ_w and ϕ_o as shown in the previous section. The same trend as before can be seen, namely that the initial distributions are smaller for better pre-separation, meaning large values of ϕ_w and ϕ_o. The oil droplet distributions at the water outlet follow the same trend as in the left plot in Figure 7, but the droplet diameter cut-off size is now almost constant. The latter is also the case for the distribution of water droplets dispersed at the oil outlet, but the distributions with respect to changes in the values of ϕ_w and ϕ_o follow now the same trend as shown in the left plot, and not the ones demonstrated in the right hand plot in Figure 7. The higher water cut clearly has an effect on the water droplet distributions at the oil outlet. The reason for this is that the horizontal residence times have almost the same value for all values of ϕ_w and ϕ_o, respectively.

Change in water level

In this section we will only present simulations for the initial production rates with low water cut, but with a change in the level of the continuous water phase. Figure 9 displays three consecutive

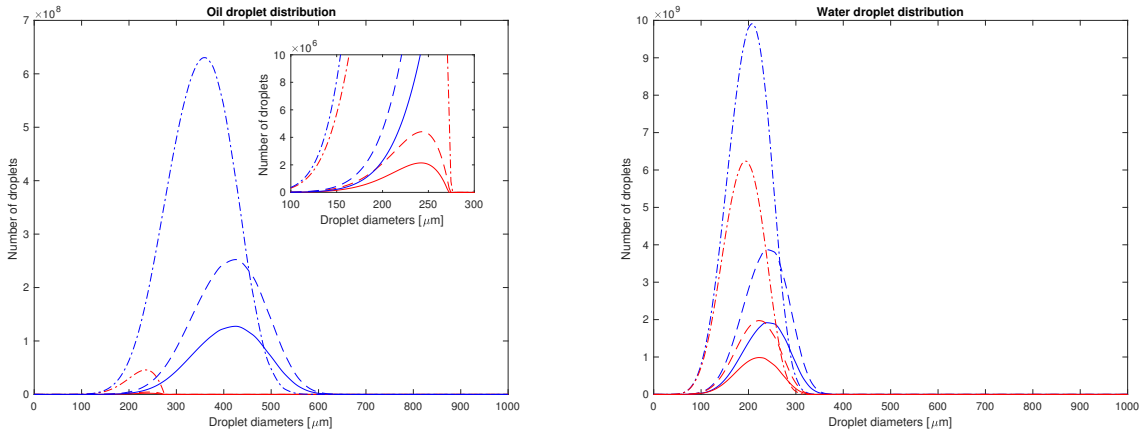

Figure 8: Initial droplet distributions (blue) and droplet distributions at the respective outlets (red) for oil droplets in water (left plot) and water droplets in oil (right plot) for three different initial separation factors ($\phi_w = \phi_o = 0.9$ (solid lines), $\phi_w = \phi_o = 0.8$ (dashed lines) and $\phi_w = \phi_o = 0.7$ (dashed-dotted lines)), high water cut

steps in the desired value of the water level, while the pressure and liquid level are held constant. It can be seen that the three PI controllers are able to control the state variables to their nominal values.

In Figure 10, the efficiencies η of oil and water removal from their respective dispersed phases are displayed. The efficiency is calculated as

$$\eta = 1 - \frac{\text{number of droplets at the respective outlet}}{\text{initially dispersed droplets at the inlet}}.$$

It can be seen that the increased water levels are beneficial for the efficiency of oil-removal from the water phase, whereas the efficiency of water-removal from the oil phase is nearly constant and no general trend can be recognized. Better pre-separation is beneficial for oil-removal from the water phase, but for water-removal from the oil phase the opposite is the case. Increasing the water level and holding the overall liquid level constant leads to a decrease in oil level and volume and an increase in water volume. With constant inflows, this leads to an increase in velocity of the continuous oil phase and a decrease in velocity for the continuous water phase.

In addition to the efficiency plots, we here present ppm-values for the cases with low water cut $\alpha = 0.135$ in Table 2 and high water cut $\alpha = 0.475$ in Table 3. For both of these cases, the initial

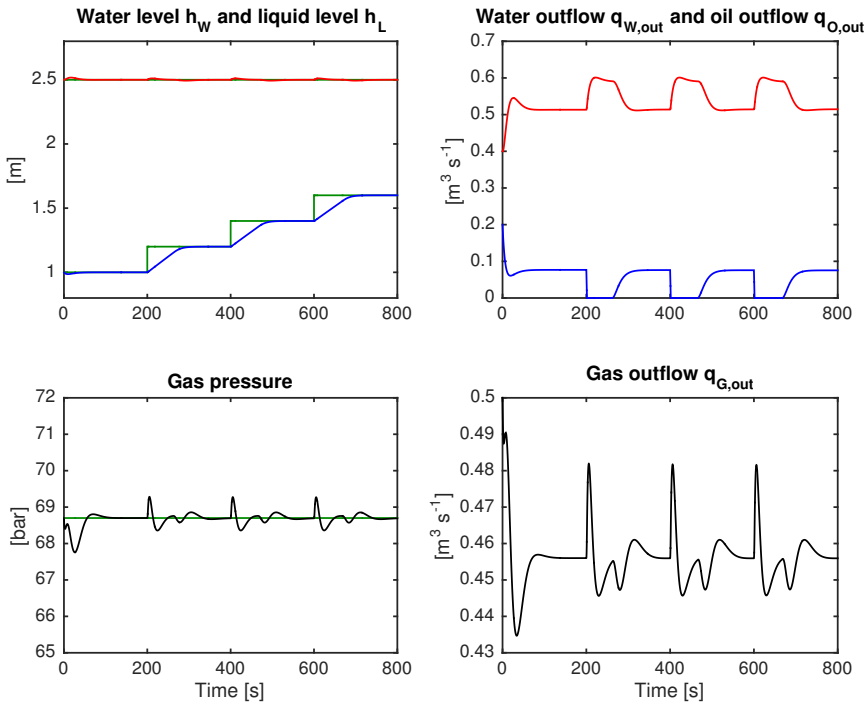

Figure 9: Left: State variables h_W (blue), h_L (red) and p (black) together with their desired values (green). Right: manipulated variables $q_{W,out}$ (blue), $q_{L,out}$ (red) and $q_{G,out}$ (black).

separation factors ϕ_o and ϕ_w as well as the water level h_W and oil level $h_O = h_L - h_W$ are subject to changes. The overall liquid level h_L is held constant.

Table 2: ppm-values for oil in water (left) and water in oil (right) at the respective outlets and for different levels as well as different pre-separation factors, $\alpha = 0.135$

		$\phi_o = \phi_w$		
		0.9	0.8	0.7
h_W	1 m	5643	38584	599999
	1.2 m	5081	35557	607083
	1.4 m	4734	33683	617540
	1.6 m	4534	32751	633140

		$\phi_o = \phi_w$		
		0.9	0.8	0.7
h_O	1.5 m	110379	192335	342895
	1.3 m	95298	165821	295452
	1.1 m	80839	140781	250581
	0.9 m	66720	116520	207100

Generally, performance of oil removal from the water-continuous phase is increased for better pre-separation, meaning large values of ϕ_o and ϕ_w. Also larger water levels h_W are beneficial for oil removal. Performance for water removal from the oil-continuous phase gets better for better pre-separation, just like in the case for oil removal from water. However, ppm-values decrease for a decrease in oil level h_O. The reason for this lies in the introduced factors, F_W and F_O, in (12),

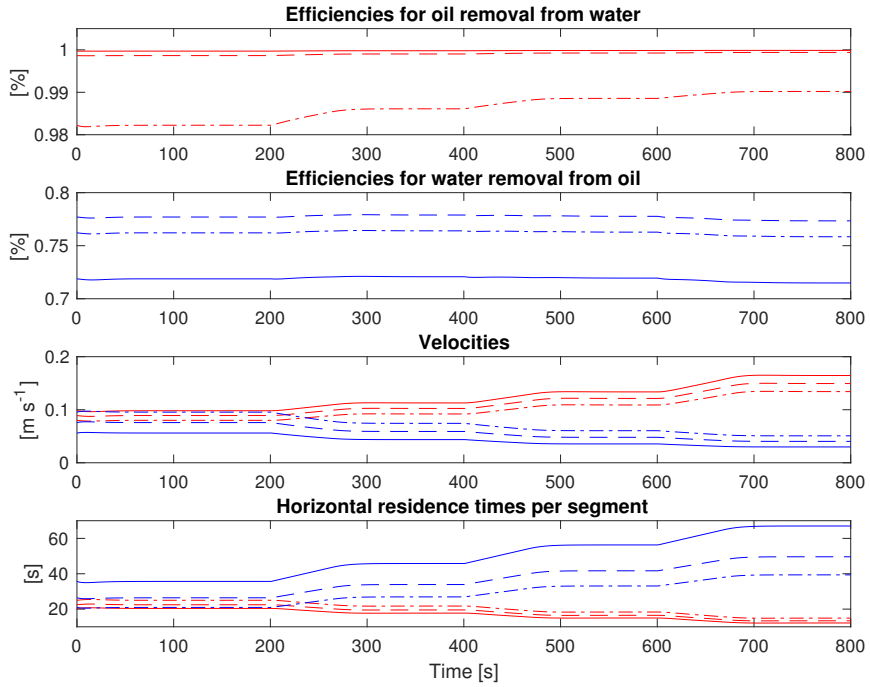

Figure 10: Two top plots: Efficiencies of removal of oil from water (red) and water from oil (blue). Third plot from top: Velocities for the continuous water (blue) and oil (red) phases. Bottom plot: Horizontal residence times for droplets in the continuous water (blue) and oil (red) phases. It holds $\phi_w = \phi_o = 0.9$ (solid), $\phi_w = \phi_o = 0.8$ (dashed) and $\phi_w = \phi_o = 0.7$ (dashed-dotted).

Table 3: ppm-values for oil in water (left) and water in oil (right) at the respective outlets and for different levels as well as different pre-separation factors, $\alpha = 0.475$

		$\phi_o = \phi_w$		
		0.9	0.8	0.7
h_W	1 m	1075	2350	28487
	1.2 m	930	2032	26362
	1.4 m	840	1839	25024
	1.6 m	787	1723	24339

		$\phi_o = \phi_w$		
		0.9	0.8	0.7
h_O	1.5 m	1031251	1987107	3936158
	1.3 m	892215	1719243	3411630
	1.1 m	755771	1456238	2884677
	0.9 m	620688	1195801	2356246

which have an influence on the initial droplet distribution. For all simulations it holds that the most realistic values are obtained for large pre-separation factors.

It must be stated that the values in Tables 2–3 highly depend on the chosen pre-separation factors ϕ_o and ϕ_w, which act as tuning parameters in the model. Furthermore, the initial distribution as calculated by the solution of the population balance model has a large influence on the ppm-values. The latter, however, is a mere assumption, since the droplet distributions can neither be

known a priori nor be measured. This leads to the conclusion that the initial distribution must be seen in context with the initial separation factors ϕ_o and ϕ_w, and the water level h_W.

Figure 11 shows the number of oil droplets in the water outlet, which are a function of the droplet diameters and time. The plot on top shows results for $\phi_w = \phi_o = 0.7$, the one in the center represents $\phi_w = \phi_o = 0.8$ and the bottom one depicts the case $\phi_w = \phi_o = 0.9$. It can be seen that by increasing the water level, both the number of droplets as well as the droplet diameter cut-off size decrease. The overall number of droplets decreases with increasing values of ϕ_w and ϕ_o, as already shown in the steady-state simulations before.

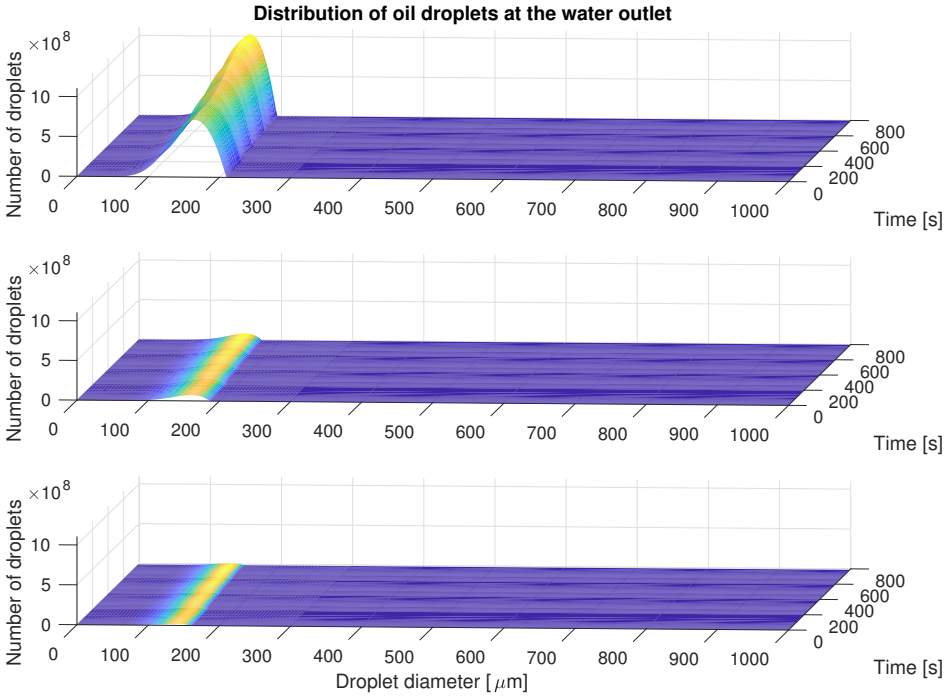

Figure 11: Number of oil droplets leaving through the water outlet for $\phi_w = \phi_o = 0.7$ (top), $\phi_w = \phi_o = 0.8$ (center) and $\phi_w = \phi_o = 0.9$ (bottom)

In Figure 12 we demonstrate the distribution of water droplets leaving through the oil outlet. The arrangement of subplots corresponds with that in Figure 11 and hence, for decreasing ϕ_{ow} and ϕ_{wo}, the overall number of droplets decreases, but not as strongly as in Figure 11. Due to the increased horizontal velocity of the continuous oil phase by an increase in water level, the number of water droplets as well as the cut-off size increase. These results correspond with the steady-state

plot on the right hand side in Figure 7.

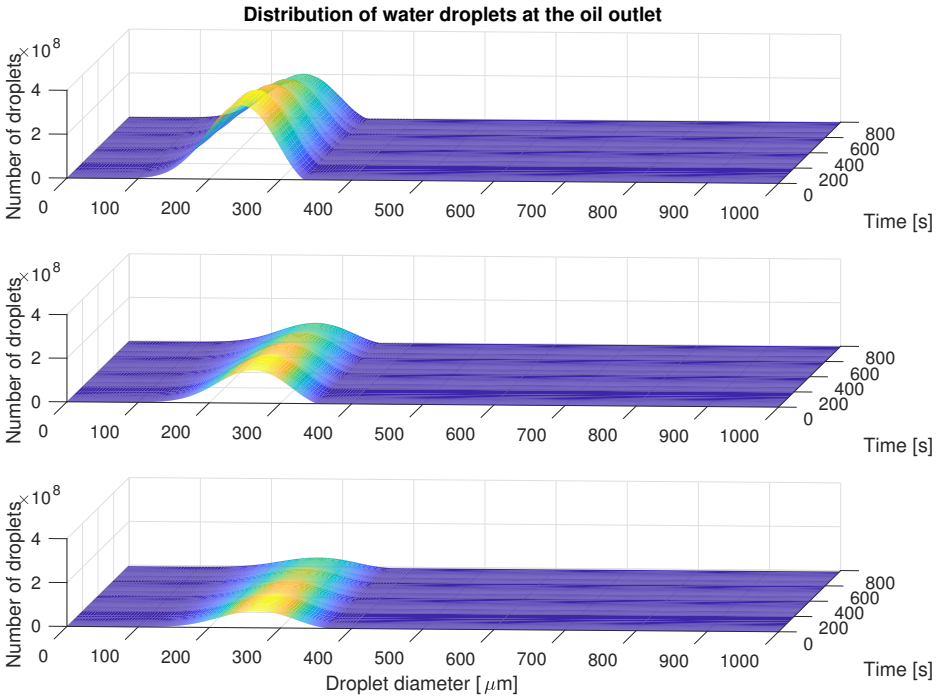

Figure 12: Number of water droplets leaving through the oil outlet for $\phi_w = \phi_o = 0.7$ (top), $\phi_w = \phi_o = 0.8$ (center) and $\phi_w = \phi_o = 0.9$ (bottom)

Observer

We next present some simulation studies demonstrating the capabilities of the disturbance estimation. Again, only simulations for initial production rates are considered, as well as fixed values for initial separation factors, namely $\phi_w = \phi_o = 0.7$. It will be shown that robustness with respect to particular disturbances in the form of white Gaussian noise can be handled satisfyingly. The simulations include the same changes in water level as introduced before. Furthermore, at $t = 400$ s and $t = 600$ s, additional step changes of $+0.1$ m^3 s^{-1} for the liquid and gas inflows are introduced, respectively.

Results without added noise

In this section, results without any added noise are presented. Figure 13 demonstrates that the water level h_W can be brought to the new nominal states and that the other states are held at their desired values after a short settling time in the beginning of the simulation. The control action can be seen in the bottom plot of Figure 13. All manipulated variables can be estimated correctly at steady state, since they are assumed to be measurable. The respective step changes in the inflows of liquid and gas at $t = 400$ s and $t = 600$ s are handled well by the controllers.

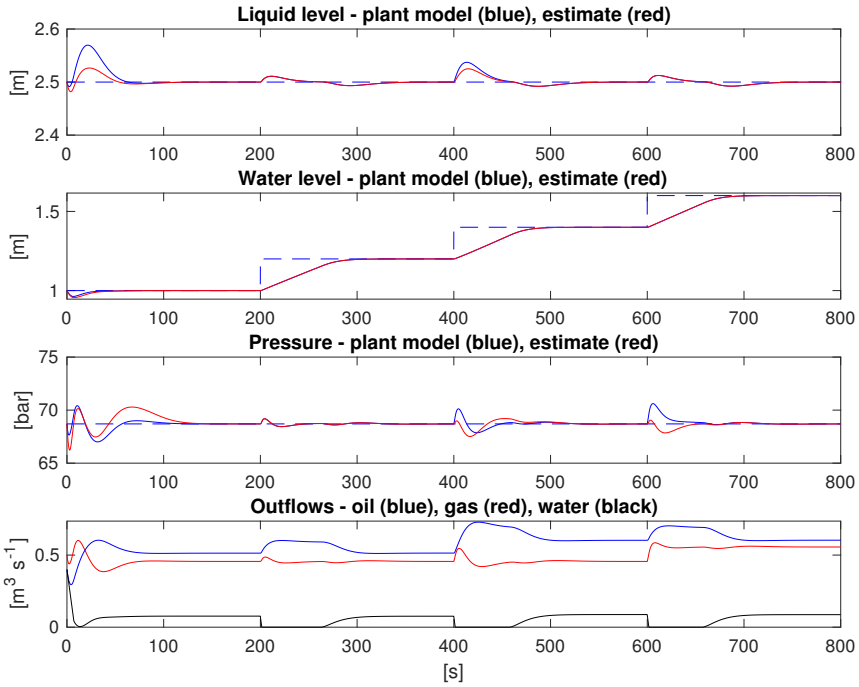

Figure 13: Top three plots: real (blue) and estimated (red) state variables together with setpoints (dashed blue); bottom plot: outflows for water (black), oil (blue) and gas (red) over time

Figure 14 shows the estimated inflows and the fraction of oil and water going into the continuous water phase. The estimated inflows $\hat{q}_{L,in}$ and $\hat{q}_{G,in}$ reach the respective nominal values of the inflows. One can see an essential difference between the estimated and real value of the parameter γ in the bottom plot, which is caused by the static droplet calculations. This static part is included in the real plant, but not in the observer model. In the simulations, the volumetric flow of oil droplets leaving the continuous water phase is larger than the volumetric flow of water droplets

leaving the continuous oil phase and hence, in steady-state, the estimated value for γ is smaller than the real value as there is a net outflow from the continuous water phase.

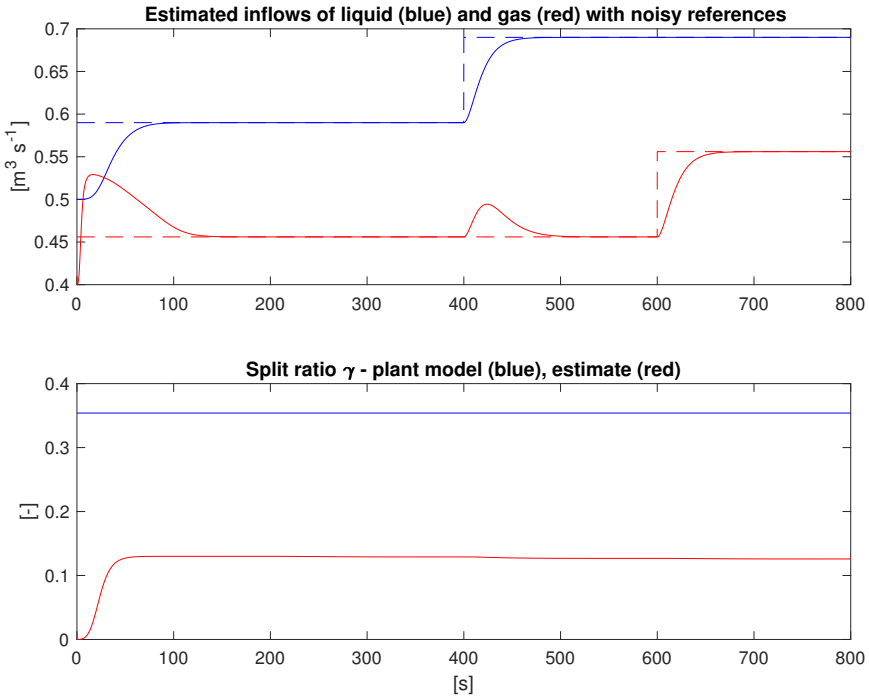

Figure 14: Top plot: real (dashed) and estimated (solid) variables, liquid inflow (blue) and gas inflow (red); center plot: zoom of top plot; bottom plot: real (blue) and estimated (red) split ratio γ

Results with added measurement, process and disturbance noise

In this section we present results for white Gaussian noise directly added to the measured variables, to the nominal values of the inflows $q_{L,in}$ and $q_{G,in}$ as well as to the time-derivatives in the observer model to regard for modeling uncertainties. Figure 15 clearly shows the added noise in the measurements, but it can be seen that the observer is able to track the real values and provide filtered signals to the controllers. As demonstrated in Figure 13 the states are held at their nominal values, again after a short settling time in the beginning of the simulation.

Figure 16, like Figure 14, shows the estimated liquid and gas inflows. Adding the measurement noise can clearly be seen in the disturbance estimates. The observer is able to track the nominal inflows correctly, despite the noisier behavior. The estimated parameter $\hat{\gamma}$ can be seen in the bottom

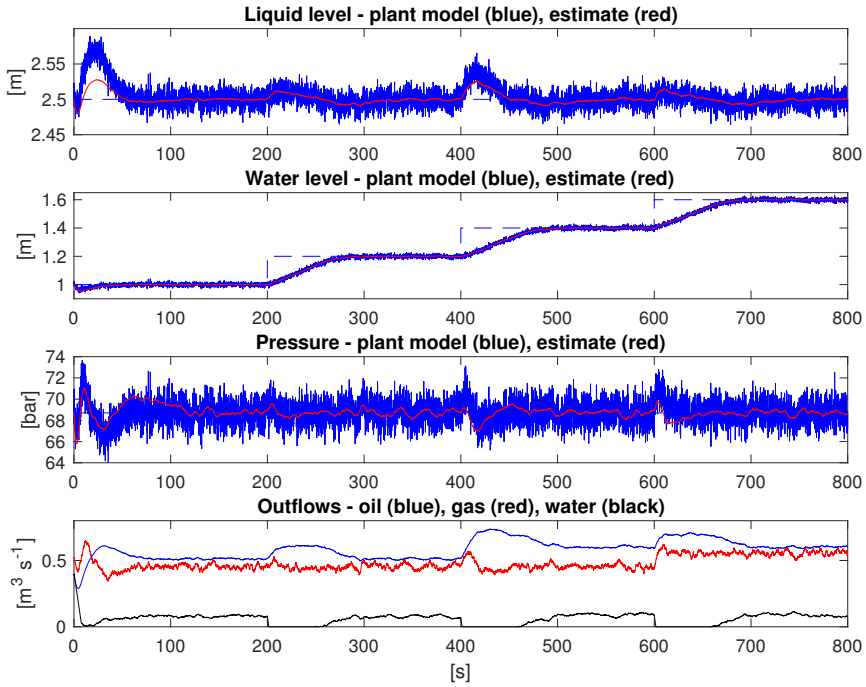

Figure 15: Top three plots: real (blue) and estimated (red) state variables together with setpoints (dashed blue); bottom plot: outflows for water (black), oil (blue) and gas (red) over time

plot and shows the same deviation from the real value as already shown in Figure 14.

Concluding Remarks

In this paper, we have presented a control- and estimation-oriented modeling approach for a three-phase gravity separator including simplified droplet balance calculations. The separator was thereby divided into three different zones, namely an inlet zone, where an instant pre-separation of oil and water occurs, an active separation zone, where droplets settle and rise due to sedimentation and creaming, and finally an outlet zone, where the gas phase as well as the continuous oil and water phases leave the separator. The latter two include dispersed water or oil droplets, which could not be removed from the bulk phases.

The dynamic states are the levels of liquid, water and the gas pressure, while the positions and the number of droplets in each volumetric segment are algebraic states. One aim of this study is to

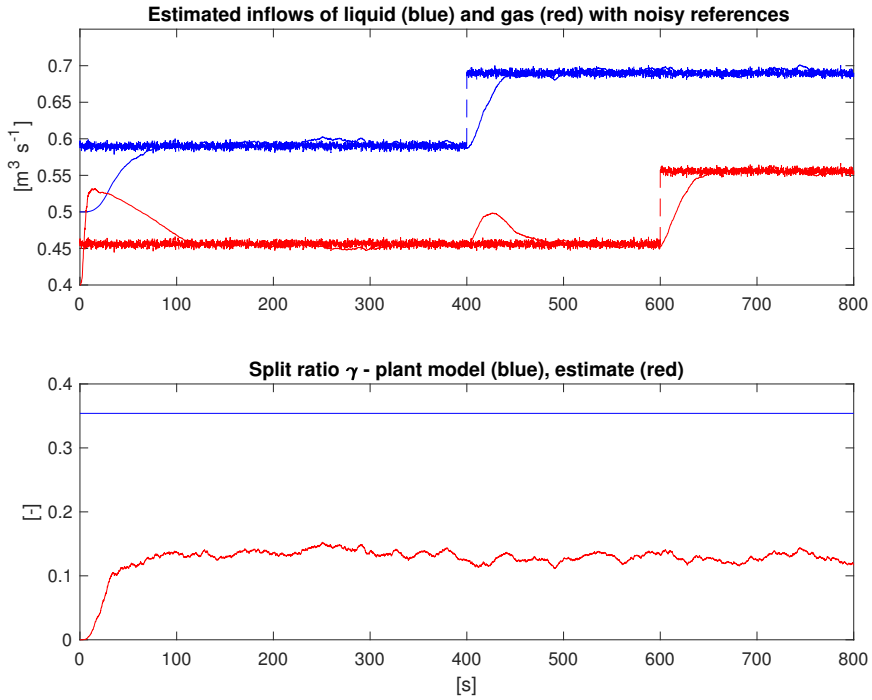

Figure 16: Top plot: real (dashed) and estimated (solid) variables, liquid inflow (blue) and gas inflow (red); center plot: zoom of top plot; bottom plot: real (blue) and estimated (red) split ratio γ

investigate the influence of different levels of water on the overall separation efficiency for water in oil, which constitutes a trade-off between horizontal and vertical residence times. The simulation results show that larger water levels are beneficial for the quality and hence purity of the water outlet stream. However, the quality of the oil outlet stream is hardly affected by changes in the oil level (which decreases as the water level increases). Initial separation in the inlet zone of the separator has a large influence on the overall quality of both outlet streams. It is demonstrated that better initial separation (large ϕ_w and ϕ_o) leads to better overall efficiencies for oil-removal from water.

The cut-off droplet sizes at the water outlet as shown in Figures 7, 8 and 11 correspond somewhat to the investigations conducted by Arntzen [3], who states that all droplets larger than roughly 210 µm are removed. This, of course, depends highly on the dimensions of the gravity separator. In order to prove its value, this study should be compared to real data. Especially the determination of the degree of initial separation in the inlet zone is very difficult to perform. Hence, the initial

separation factors ϕ_w and ϕ_o could serve as tuning parameters to fit the model to real data.

Furthermore, we presented a virtual monitoring approach for the developed gravity separator model in this paper. A cascaded dual observer design based upon two Extended Kalman Filters in an alternative formulation with forgetting factor was used to filter the signals of the measured state variables and to obtain estimates for the disturbance variables (liquid and gas inflows) acting on the process as well as the effective split ratio of oil and water entering the continuous water phase.

The performance of the Extended Kalman Filter together with PI controllers is presented for different simulation cases. These include tracking of step changes in the desired water level as well as step disturbances in the inflows of liquid and gas. In addition, white noise was added to the three measured state variables, to the disturbance variables and as process noise to the state derivatives. The simulation results show that the proposed control and estimation structure is capable of estimating smoother values of the state variables and utilize these in the controllers. In addition, the nominal values of the disturbance variables are estimated correctly.

One drawback of the estimation and control structure is that the split ratio γ of oil and water entering the continuous water phase cannot be estimated correctly. This is caused by the fact that there is a net outflow of oil leaving the continuous water phase into the continuous oil phase due to steady-state separation calculations. This static part of the model is included in the plant, but not in the observer. Hence, the estimated value $\hat{\gamma}$ represents the effective split ratio in steady-state conditions including separation.

The suggested estimation and control structure is not limited to separation systems in the oil and gas industry, but can be implemented in all kinds of in- and outflow systems. Nevertheless, in order to prove its value and implementability, it should be tested on a real plant, preferably for a single-phase application in the beginning.

Future work can include further investigation of the deviation between the split ratio γ and its estimated value $\hat{\gamma}$ and how to utilize this information in a real application. The split ratio itself is not determinable, but a qualitative interpretation of its estimate could lead to a better understanding of the separation inside the separator. In addition, more sophisticated control structures incorporating

the disturbance estimates in a feedforward-manner with disturbance compensation by e.g. state-feedback control could be designed.

Appendix A: Parameters

L	Length of active separation zone	10 m
M_G	Molar mass of the gas	0.01604 kg mol^{-1}
N_S	Number of segments	5
r	Radius of the separator	1.65 m
R	Universal gas constant	8.314 $\frac{\text{kg m}^2}{\text{s}^2\ \text{mol K}}$
T	Temperature	328.5 K
V_{Sep}	Volume of active separation zone	85.53 m^3
g	Gravitational acceleration	9.8 m s^{-2}
$q_{G,in}$	Volumetric inflow of gas	0.456 m^3 s^{-1}
$q_{L,in}$	Volumetric inflow of liquid	0.59, 0.73 m^3 s^{-1}
α	Water cut of the liquid inflow	0.135, 0.475
β	Oil cut of the liquid inflow	0.865, 0.525
γ	Split ratio	0.354
μ_O	Dynamic viscosity oil	0.001 kg (s m)$^{-1}$
μ_W	Dynamic viscosity water	0.0005 kg (s m)$^{-1}$
ρ_G	Density of gas	49.7 kg m^{-3}
ρ_O	Density of oil	831.5 kg m^{-3}
ρ_W	Density of water	1030 kg m^{-3}
ϕ_w	Initial separation factor for water	0.7, 0.8, 0.9
ϕ_o	Initial separation factor for oil	0.7, 0.8, 0.9

Observer tunings:
$$R_{O_1} = 10^0 \quad , \quad \lambda_{O_1} = 10^{-1}$$
$$R_{O_2} = \text{diag}\left(10^0,\ 10^4\right) \quad , \quad \lambda_{O_2} = 10^{-1}$$

Appendix B: Sensitivity analysis

In this section we investigate how the solution converges with respect to the chosen discretization of the droplet size classes for one case example with $\phi_o = \phi_w = 0.9$. We conducted this investigation with 5, 10, 20, 50, 100, 250 and 500 droplet size classes (see Figure 17) and a metric, where the fractions of oil and water at the respective water- and oil-continuous outlets (see Figure 18) are compared. As can be seen, from around $50-100$ droplet size classes there are no big improvements with respect to solution accuracy and hence we believe that by choosing 500 droplets size classes we obtain a sufficiently accurate solution.

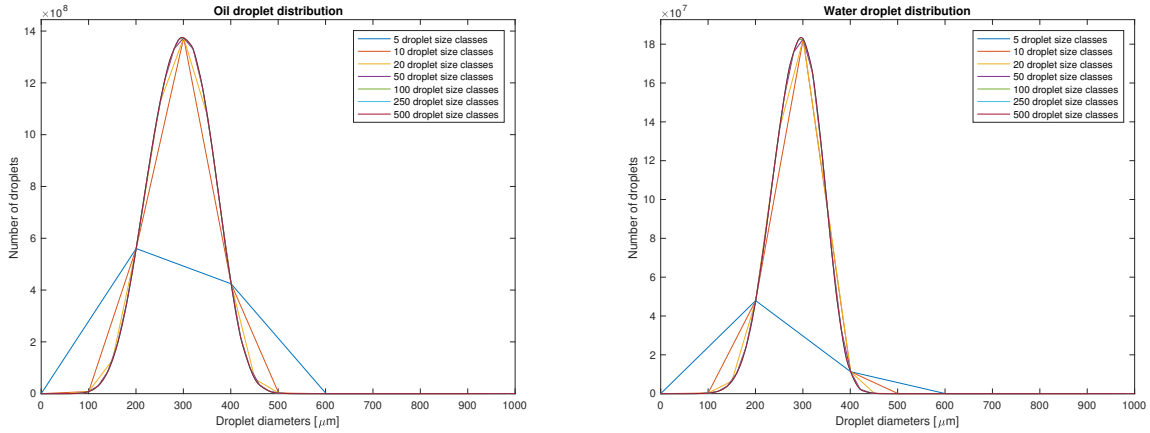

Figure 17: Different resolutions of the droplet size class for oil and water droplets

Acknowledgement

The authors gratefully acknowledge financial support from the Norwegian Research Council in the project SUBPRO (Subsea Production and Processing).

References

(1) Sayda, A. F.; Taylor, J. H. Modeling and Control of Three-Phase Gravity Separators in Oil Production Facilities. Proceedings of the American Control Conference. New York City,

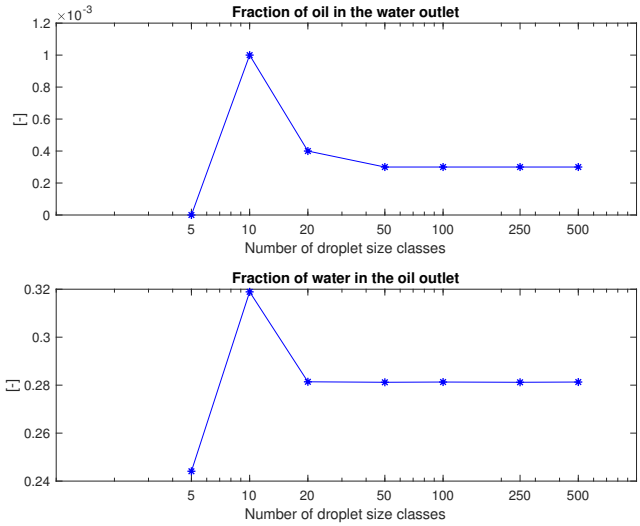

Figure 18: Sensitivity analysis over the resolution of the droplet size classes

USA, 2007; pp 4847–4853.

(2) Hallanger, A.; Michelsen, C.; Soenstaboe, F.; Knutsen, T. A Simulation Model for Three-Phase Gravity Separators. Proceedings of the SPE Annual Technical Conference and Exhibition. Denver, CO, USA, 1996; pp 695–706.

(3) Arntzen, R. Gravity Separator Revamping. Ph.D. thesis, Norwegian University of Science and Technology, Trondheim, Norway, 2001.

(4) Hansen, E. W. M.; Heitmann, H.; Lakså, B.; Ellingsen, A.; Østby, O.; Morrow, T. B.; Dodge, F. T. Fluid Flow Modelling of Gravity Separators. Proceedings of the 5th International Conference on Multi-Phase Production. Cannes, France, 1991; pp 364–380.

(5) Hansen, E. W. M.; Heitmann, H.; Lakså, B.; Løes, M. Numerical Simulation of Fluid Flow Behaviour Inside, and Redesign of a Field Separator. Proceedings of the 6th International Conference on Multi-Phase Production. Cannes, France, 1993; pp 117–129.

(6) Laleh, A. P.; Svrcek, W. Y.; Monnery, W. D. Computational Fluid Dynamics-Based Study of an Oilfield Separator - Part I: A Realistic Simulation. *Oil Gas Facil.* **2012**, *1*, 57–68.

(7) Backi, C. J.; Skogestad, S. A simple dynamic gravity separator model for separation efficiency evaluation incorporating level and pressure control. Proceedings of the American Control Conference. Seattle, USA, 2017; pp 2823–2828.

(8) Jaworski, A. J.; Meng, G. On-line measurement of separation dynamics in primary gas/oil/water separators: Challenges and technical solutions – A review. *J. Pet. Sci. Eng.* **2009**, *68*, 47–59.

(9) Meribout, M.; Habli, M.; Al-Naamany, A.; Al-Busaidi, K. A New Ultrasonic-based Device for Accurate Measurement of Oil, Emulsion, and Water Levels in Oil Tanks. Proceedings of the Instrumentation and Measurement Technology Conference. Como, Italy, 2004; pp 1942–1947.

(10) McClimans, O. T.; Fantoft, R. Status and New Developments in Subsea Processing. Proceedings of the Offshore Technology Conference. Houston, TX, USA, 2006; pp 731–740.

(11) Bukhari, S. F. A.; Yang, W. Multi-interface Level Sensors and New Development in Monitoring and Control of Oil Separators. *Sensors* **2006**, *6*, 380–389.

(12) Hjertaker, B. T.; Johansen, G. A.; Jackson, P. Level measurement and control strategies for subsea separators. *J. Electron. Imaging* **2001**, *10*, 679–689.

(13) van der Tuuk Opedal, N.; Sørland, G.; Sjöblom, J. Methods for Droplet Size Distribution Determination of Water-in-Oil Emulsions using Low-Field NMR. *Diffus. Fundam.* **2009**, *9*, 1–29.

(14) Bennett, M. A.; Williams, R. A. Monitoring the operation of an oil/water separator using impedance tomography. *Miner. Eng.* **2004**, *17*, 605–614.

(15) Durdevic, P.; Hansen, L.; Mai, C.; Pedersen, S.; Yang, Z. Cost-Effective ERT Technique for Oil-in-Water Measurement for Offshore Hydrocyclone Installations. Proceedings of the 2nd

IFAC Workshop on Automatic Control in Offshore Oil and Gas Production. Florianópolis, Brazil, 2015; pp 153–159.

(16) Pedersen, S.; Mai, C.; Hansen, L.; Durdevic, P.; Yang, Z. Online Slug Detection in Multi-Phase Transportation Pipelines Using Electrical Tomography. Proceedings of the 2nd IFAC Workshop on Automatic Control in Offshore Oil and Gas Production. Florianópolis, Brazil, 2015; pp 165–170.

(17) Li, H.; Mohan, R. S.; Marrelli, J.; Wang, S. Differential Dielectric Sensor Model and Its Applications for Water and Oil Flow. Proceedings of the ASME International Mechanical Engineering Congress & Exposition. Vancouver, BC, Canada, 2010; pp 147–154.

(18) Luggar, R. D.; Key, M. J.; Morton, E. J.; Gilboy, W. B. Energy dispersive X-ray scatter for measurement of oil/water ratios. *Nucl. Instrum. Methods Phys. Res., Sect. A* **1999**, *422*, 938–941.

(19) Thorn, R.; Johansen, G.; Hjertaker, B. Three-phase flow measurement in the petroleum industry. *Meas. Sci. Technol.* **2013**, *24*.

(20) Bothamley, M. Gas/Liquid Separators - Quantifying Separation Performance - Parts 1–3. *Oil Gas Facil.* **2013**, *2*, 21–29, 35–47, 34–47.

(21) Laleh, A. P.; Svrcek, W. Y.; Monnery, W. D. Computational Fluid Dynamics-Based Study of an Oilfield Separator - Part II: An Optimum Design. *Oil Gas Facil.* **2013**, *2*, 52–59.

(22) Richardson, J. F.; Zaki, W. N. The sedimentation of a suspension of uniform spheres under conditions of viscous flow. *Chem. Eng. Sci.* **1954**, *8*, 65–73.

(23) Kharoua, N.; Khezzar, L.; Saadawi, H. CFD Modelling of a Horizontal Three-Phase Separator: A Population Balance Approach. *Am. J. Fluid Dyn.* **2013**, *3*, 101–118.

(24) Jakobsen, H. A. *Chemical Reactor Modeling*; Springer-Verlag: Berlin Heidelberg, 2008.

(25) Grimes, B. A. Population Balance Model for Batch Gravity Separation of Crude Oil and Water Emulsions. Part I: Model Formulation. *J. Dispersion Sci. Technol.* **2012**, *33*, 578–590.

(26) Grimes, B. A.; Dorao, C. A.; Opedal, N. V. D. T.; Kralova, I.; annd J. Sjöblom, G. H. S. Population Balance Model for Batch Gravity Separation of Crude Oil and Water Emulsions. Part II: Comparison to Experimental Crude Oil Separation Data. *J. Dispersion Sci. Technol.* **2012**, *33*, 591–598.

(27) Prince, M. J.; Blanch, H. W. Bubble coalescence and break-up in air-sparged bubble columns. *AIChE J.* **1990**, *36*, 1485–1499.

(28) Chesters, A. The modeling of coalescence processes in fluid liquid dispersions - A review of current understanding. *Chem. Eng. Res. Des.* **1991**, *69*, 259–270.

(29) Coulaloglou, C. A.; Tavlarides, L. L. Description of interaction processes in agitated liquid-liquid dispersions. *Chem. Eng. Sci.* **1977**, *32*, 1289–1297.

(30) Vankova, N.; Tcholakova, S.; Denkov, N. D.; Vulchev, V. D.; Danner, T. Emulsification in turbulent flow: 2. Breakage rate constants. *J. Colloid Interface Sci.* **2007**, *313*, 612–629.

(31) Skogestad, S. Simple analytic rules for model reduction and PID controller tuning. *J. Process Control* **2003**, *13*, 291–309.

(32) Backi, C. J.; Skogestad, S. Virtual inflow monitoring for a three phase gravity separator. Proceedings of the 1st IEEE Conference on Control Technology and Applications. Kohala Coast, Hawaii, USA, 2017; pp 1499–1504.

(33) Johnstone, R. M.; Johnson, C. R.; Bitmead, R. R.; Anderson, B. D. Exponential convergence of recursive least squares with exponential forgetting factor. Proceedings of the 21st IEEE Conference on Decision and Control. Orlando, Florida, USA, 1982; pp 994–997.

(34) Hammouri, H.; De Leon Morales, J. Observer synthesis for state-affine systems. Proceedings

of the 29th IEEE Conference on Decision and Control. Honululu, Hawaii, USA, 1990; pp 784–785.

(35) Haring, M. A. M. Extremum-seeking control: convergence improvements and asymptotic stability. Ph.D. thesis, Norwegian University of Science and Technology, Trondheim, Norway, 2016.

Graphical TOC Entry